



Pareto-optimal analysis of Zn-coated Fe in the presence of dislocations using genetic algorithms

Pankaj Rajak^a, Sudipto Ghosh^a, Baidurya Bhattacharya^b, Nirupam Chakraborti^{a,*}

^a Department of Metallurgical & Materials Engineering, Indian Institute of Technology, Kharagpur 721 302, India

^b Department of Civil Engineering, Indian Institute of Technology, Kharagpur 721 302, India

ARTICLE INFO

Article history:

Received 21 February 2012

Received in revised form 23 March 2012

Accepted 1 May 2012

Available online 1 June 2012

Keywords:

Fe–Zn system

Molecular dynamics

Artificial neural network

Genetic algorithm

Multi-objective optimization

Grain boundary

Dislocation

ABSTRACT

To design a coating that will absorb maximum energy prior to failure with minimum deformation, the shearing process of polycrystalline Zn coated Fe is simulated in the presence of dislocations, using molecular dynamics. The results fed to an Evolutionary Neural Network generated the meta-models of objective functions required in the subsequent Pareto-optimization task using a Multi-objective Genetic Algorithm. Similar calculations conducted for single crystals, and also in the absence of dislocations, are compared and analyzed.

© 2012 Elsevier B.V. All rights reserved.

1. Introduction

An assembly of Fe and Zn and thereafter the phases in a Zn coated layer were studied in two of our earlier investigations [1,2] by coupling molecular dynamics (MD) with a genetic algorithm based [3] bi-objective optimization procedure [4–7]. A more realistic simulation would however call for studying the polycrystals in the presence of dislocations. This necessitated a series of additional simulations and the outcome is summarized in this communication.

2. Methodology

The idea behind this study is to design a coated assembly at the molecular level, which would, at some prescribed situation of failure, tend to show a minimum amount shear induced deformation (γ) after a maximum amount of energy absorption (ΔE) relative to some reference point. The optimization task therefore was:

$$\left. \begin{array}{l} \text{maximize } \Delta E_f \\ \text{minimize } \gamma_f \end{array} \right\} \quad (1)$$

* Corresponding author. Tel.: +91 9434009164.

E-mail address: nchakrab@gmail.com (N. Chakraborti).

where the subscript f denotes a predefined failure point, taken conveniently as the relative interlayer displacement exceeding the lattice spacing of Zn–Zn, as detailed earlier [1,2]. The decision variables are as listed in Table 1. Since these two objectives are mutually conflicting, together they would never be able to attain their individual best levels. This leads to a Pareto-optimal problem [8], studied extensively in recent times [9] where the singular optimum solution, generally encountered in case of conventional single objective tasks, is replaced by a Pareto-optimal set, in which the members represent the best possible trade-offs between the objectives. Pareto-frontier, the locus of the members in the Pareto-set, denotes the boundary between the feasible and infeasible solution space and no feasible solution could be better than any member of in this frontier in terms of one or more objectives, while remaining equally good in terms of the rest. Mathematically Pareto-optimality can be defined as follows [8,9]:

For a decision variable vector $x = (x_1, x_2, \dots, x_n)^T$; $x \in S$, where S denotes the *feasible solution space*, a subset of the *decision variable space* \mathcal{R}^n , if we attempt to minimize the corresponding vector of objective functions $f(x) = (f_1(x), f_2(x), \dots, f_k(x))^T$; where $k \geq 2$ and each objective function $f_i: \mathcal{R}^n \rightarrow \mathcal{R}$, then a *decision vector* $\tilde{x} \in S$ is *Pareto-optimal* if there exist no other decision vector $x \in S$ for which $f_i(x) \leq f_i(\tilde{x})$ for all $i = 1, \dots, k$ and at least for one i $f_i(x) < f_i(\tilde{x})$. Similarly, an objective vector $\tilde{z} \in Z$ is Pareto-optimal if the decision vector corresponding to it is Pareto-optimal. In recent times

Table 1
Input variable list for molecular dynamics simulation.

Polycrystalline Fe–Zn system		Single crystalline Fe–Zn system	
Shear velocity (m/s)	10, 30, 50	Shear velocity (m/s)	10, 30, 50
Coating thickness (Å)	30, 40, 56	Coating thickness (Å)	30, 40, 56
Grain size (Fe–Zn) (Å)	84–78, 102–92, 110–100	Fe–Zn interfacial orientation	0°, 2.5°, 5°, 7.5°, 10°, 20°, 30°
Grain orientation (Fe–Zn)	Low–Low, Low–High, High–Low, High–High		
(High angle grain boundary: $\geq 20^\circ$; low angle grain boundary: $\leq 10^\circ$)			
Time step	0.5 fs		

All simulations were for (0001) Zn over (100) Fe.
Periodic boundary condition in all directions.

genetic algorithms are being very efficiently used to compute Pareto-optimality [9].

3. Computing strategy

In this study shear deformations for both polycrystalline and single crystalline Fe–Zn assemblies were first simulated through molecular dynamics using LAMMPS [10]. Dislocations were introduced in these assemblies through uniaxial tensile deformation prior to shearing. This aspect of the present work makes it more realistic and significantly different from its predecessors [1,2] where no such attempts were made. Further details are provided in Fig. 1.

To reduce the computing burden of the optimization process the data from the MD simulations were utilized to construct meta-models for both γ and ΔE . An Evolutionary Neural Network (EvoNN) developed and used extensively in our earlier studies [1,2,4,11,12] was utilized for that. The genetic and evolutionary approach used in this study and our earlier works [1,2] requires to process a population of probable solutions from generation to generation till convergence. Thus, in contrast with the gradient based optimization strategies, here we require to evaluate the objective functions for each member of the population and that too in every generation. Attempting this through direct MD simulations in each case requires a huge computing power and the simulations done without a massive parallelization quickly tend to go out of hand. It's however, a totally different story when the direct MD simulations are replaced by objective function evaluations through a meta-model: there the computing time drastically reduces. For example, in a Windows Server 2003 R2 environment of a single processor machine with Intel(R) Xeon(R) CPU (E5420 @ 2.50 GHz) with 3.25 GB of RAM, a single MD simulation for the higher velocities would require anywhere between 9.7 and 13.89 h to execute, and here for the construction of a meta-model, on the average, we needed about a hundred of such simulations. For some of the higher velocities used in this study, a second processor was needed to finish the calculations within a comparable amount of time. Running the optimization task in an evolutionary

environment for a moderately decent population size of hundred, for hundred generations without the meta-model, will require 10,000 of such MD runs, leading to about two orders of magnitude increase in the computing time. The task therefore, is to come up with a meta-model that would faithfully represent the basic trends in the MD data. Unlike the conventional Neural Nets, EvoNN uses a flexible architecture and evolves using a Multi-objective Genetic Algorithm, as a Pareto tradeoff between the complexity of the network and the accuracy of training. This led to the Pareto-frontiers shown in Fig. 2 where each empty diamond represents a separate optimized neural net, out of which one in each case, marked as solid diamonds, was selected by applying a corrected Akaike Information Criteria [6]. Further details are available elsewhere [4,6].

Using a Predator–prey bi-objective Genetic Algorithm [4] the meta-models were utilized for generating the Pareto-frontiers between γ and ΔE . The computational steps are further elaborated in Fig. 3 and the input variables for MD simulations are summarized in Table 1. Although attempts were made to use realistic parameters as far as possible, the value of shear velocity remained a bit above normal, so that the MD simulations do not require prohibitively large time steps to reach the failure level.

Here Fe and Zn polycrystals were generated by first creating large cubic shaped structures for them with crystallographic orientation of (100) for Fe and (0001) for Zn. These crystals are then rotated by different angles, between 2.5° and 60°, along Y axis in X–Z plane, creating different configurations. Next, a hexagon was removed from these structures. Different grains of a polycrystalline structure were created by placing such hexagons adjacent to each other so that they make tilt boundaries amongst themselves.

Both high ($\geq 20^\circ$) and low ($\leq 10^\circ$) angle grain boundaries were created following this procedure detailed elsewhere [13–16].

Energy minimization of these polycrystals was conducted using conjugate-gradient method. Subsequently they were stabilized as NVE ensemble for 10,000 time steps and then under NPT ensemble for another 10,000 time steps. A typical polycrystal of Fe is shown in Fig. 4 along with the equilibrated structure.

Stabilized Zn polycrystals were placed over stabilized Fe to create the Fe–Zn system with various grain orientations. This assembly was again stabilized as NPT ensemble and subjected to shear deformation. This equilibrated system was subjected to uniaxial tensile deformation at a constant engineering strain rate ($5 \times 10^8 \text{ sec}^{-1}$) for 1.5 ps as NPT ensemble in order to generate defects and dislocations from the grain boundaries. The system was then again stabilized as an NPT ensemble before subjecting it to shear force under NPT conditions.

The shear force was introduced to the equilibrated assembly by setting a few atoms of top layer in motion with constant velocity, holding some atoms in the bottom layer fixed. It was done under an NPT ensemble and the shearing effects gradually propagated from layer to layer. The entire system was assumed to be under plain strain condition. When the relative displacement of any layer above

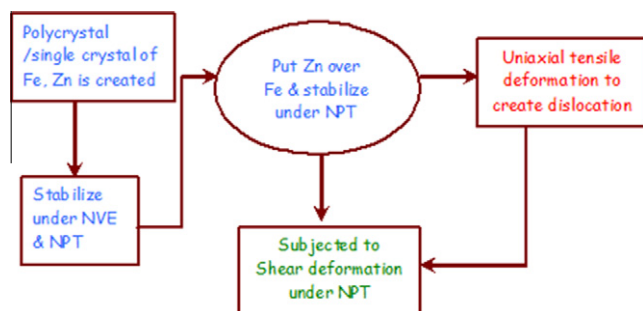


Fig. 1. Molecular dynamics simulation of Fe–Zn system.

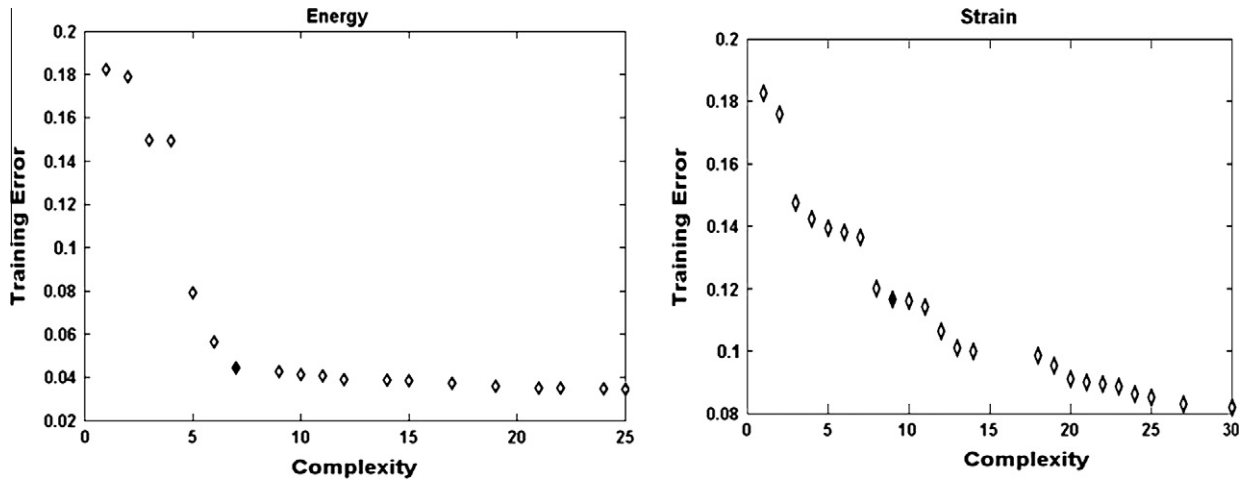


Fig. 2. Tradeoff between training error and complexity for the optimized EvoNN networks.

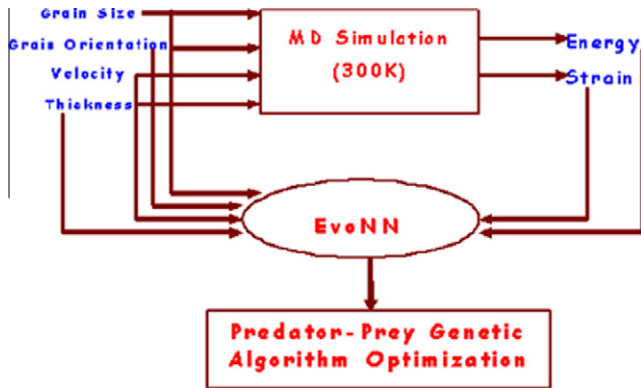


Fig. 3. Computational flow chart of Polycrystalline Fe-Zn System.

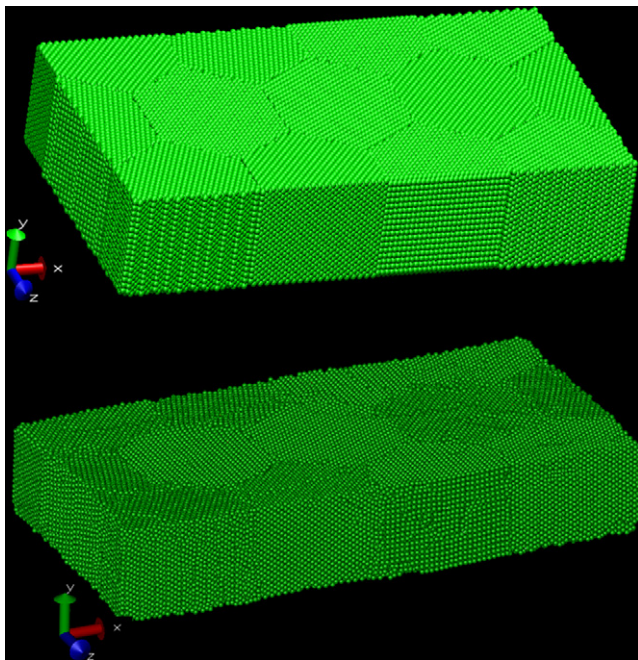


Fig. 4. Initial (top) and equilibrated structure of polycrystalline Fe.

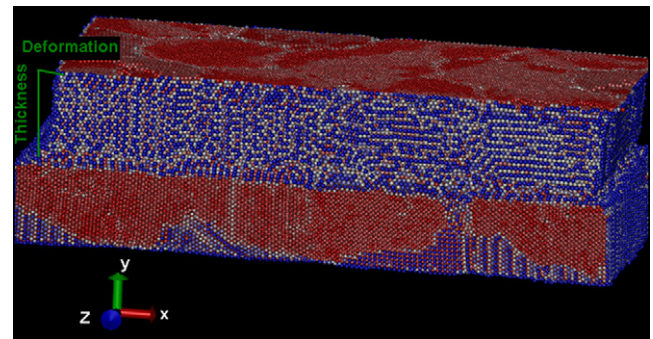


Fig. 5. Fe-Zn assembly of high angle grain orientation at the onset of failure.

was identified from the corresponding RMS displacement (δ_{rms}) vs. time plot. Further details are provided elsewhere [1,2]. A typical structure of Zn coated Fe, both with high angle grain orientations, is shown in Fig. 5 at the onset of shear deformation.

The energy of the system at the onset of failure provided the shear energy absorbed up to the point of failure, and enabled computing of the first objective function. The energy needed for failure was taken as the difference between the energy at the failure point and that at the end of initial equilibration, when the shearing process started.

The shear strain at failure (γ), the second objective, was computed as the ratio of deformation of the top layer by thickness, as explained schematically in Fig. 5.

For the single crystals the initial configuration was created by placing (0001) Zn crystal over (100) Fe crystal, keeping the interfacial orientation as 0° . To create structure with different interfacial orientation at the Fe-Zn interface, the Zn crystal was rotated with respect to Fe to create the interfacial orientations listed in Table 1. These structures were then stabilized and deformed, following the scheme outlined in Fig. 1. Some instances of stabilized and deformed structures are presented in Figs. 4 and 5. The data generated from MD simulations were fed into EvoNN for creating meta-models for γ and ΔE , considering polycrystalline systems with and without dislocations, along with the single crystalline system. Typical models for both ΔE and γ are shown in Fig. 6.

4. Analyses of results

The Pareto-frontiers of all three systems are compared in Fig. 7. All the Pareto-solutions correspond to a low shear velocity of

the interface exceeded the value of 2.87 \AA , the lattice parameter of Fe, the onset of shear failure was assumed. This point of shear failure

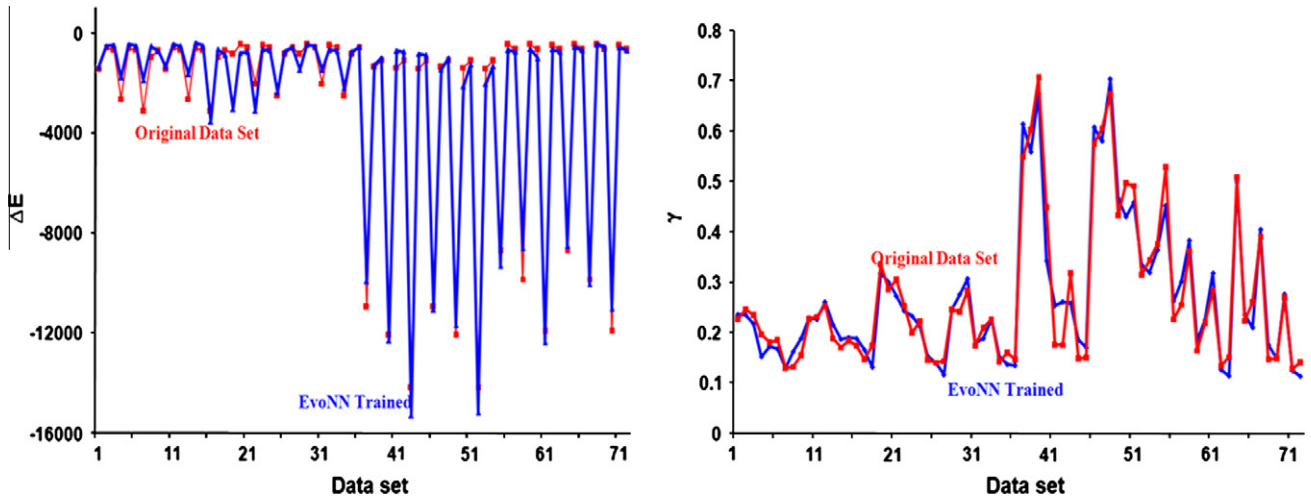


Fig. 6. Performance of EvoNN meta-models for polycrystals without dislocation. The values refer to the predefined failure point.

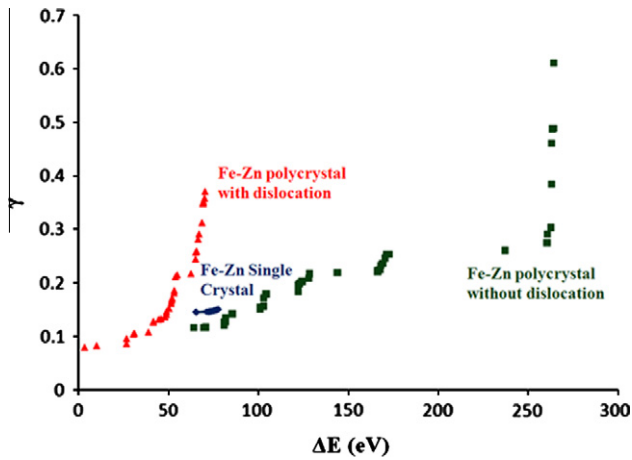


Fig. 7. Computed Pareto-frontiers. The values refer to the predefined failure point.

10 m/s. Deformations at higher velocities would impart larger strain in most levels of energy absorption, leading to solutions dominated by the ones present in the Pareto-frontier. Expectedly, the Pareto-solutions obtained for the Fe–Zn polycrystal with dislocations are dominated by those without it. The dislocations set into motion by any value of ΔE led to a higher value of γ than the dislocation free polycrystals, leading to inferior solutions in terms of the present objectives. The Pareto-solutions were further analyzed in the variable space. The results are summarized in Table 2. In this table the maximum numbers in a given category are indicated in boldfaced italics.

A careful examination of Table 2 reveals that in the absence of dislocations in polycrystals most of the Pareto-solutions came from low–low (Fe–Zn) grain orientations, while in the presence of dislocations most were from high–high grain boundary orientations. Possible phenomenon underlying such trend is as follows. High angle grain boundaries are better emitter of dislocations. Thus in the absence of dislocations, presence of high angle grain

Table 2
Parameters of Pareto-solutions.

Polycrystal without dislocation based upon grain size				
Grain boundary orientation (Fe–Zn)	Grain size (Å)	Coating thickness (Å)	Number of Pareto values	# Pareto-solutions for a grain orientation
Low–Low	84	55	4	27
	94	35	1	
	105	55	22	
Low–High	84	55	6	15
	94	45	1	
	94	45	1	
High–Low	105	55	7	5
	94	35	1	
	94	45	1	
High–High	94	35	3	3
	84	55	1	
94	45	2		
Polycrystal without dislocation based upon ΔE				
ΔE	Grain boundary orientation (Fe–Zn)	Grain size	Coating thickness	# Pareto solutions
<100 eV	Low–Low	84	55	2
		94	35	1
	Low–High	105	55	4
		105	55	3

(continued on next page)

Table 2 (continued)

Grain boundary orientation (Fe–Zn)	Grain size (Å)	Coating thickness (Å)	Number of Pareto values	# Pareto-solutions for a grain orientation
100–200 eV	High–Low	94	35	1
		94	55	1
	Low–Low	84	55	2
		105	55	12
		84	55	3
	Low–High	94	45	1
		94	55	1
		105	55	3
	High–Low	84	55	1
		94	45	2
	High–High	94	45	1
		94	55	2
>200 eV	Low–Low	105	55	6
		35	55	3
	Low–High	105	55	1
Polycrystal with dislocation based upon grain size				
Grain boundary orientation (Fe–Zn)	Grain size	Coating thickness	Number of Pareto values	# Pareto-solutions for a grain orientation
Low–High	84	55	4	6
	105	55	2	
High–High	84	45	1	
		55	13	
	94	35	3	
		45	4	
		55	5	
105	55	3	29	
High–Low	94	45	1	1
Polycrystal with dislocation based upon ΔE				
ΔE	Grain boundary orientation (Fe–Zn)	Grain size	Coating thickness	# Pareto solutions
>40 eV	High–High	105	105	1
		84	55	4
	Low–High	105	55	2
40–60 eV	High–High	84	45	1
		84	55	13
		94	55	1
		105	55	2
>60 eV	High–High	94	35	3
		94	45	4
		94	55	4
	High–Low	94	45	1
		94	45	1
Single crystal on the basis of ΔE				
ΔE	Fe–Zn interfacial orientation	Coating thickness	Number of Pareto values	
<66 eV	<1°	56	2	
>70 eV	25–30°	56	33	

boundaries result in easier shear straining and thus lower absorption of energy. Consequently, in the absence of dislocations, low–low boundaries which will require higher absorption energy would dominate. On the other hand in the presence of dislocations or pre-strain, further emission of dislocation by high–high boundary possibly hardens the polycrystal resulting in higher absorption of energy as compared to low angle boundaries. Thus the observed trend is due to the fact that a polycrystal deforms most easily or absorbs minimum energy at an optimum level of dislocation density.

5. Concluding remarks

As a concluding remark: although Genetic and Evolutionary algorithms are now being extensively used for studying various assemblies at the atomic level [17–19] and also for designing steels of newer properties and compositions [20], the bi-objective

meta-modeling strategy, as adopted in this work and our earlier studies of this system [1,2] is still at the cutting edge, and warrants further exploitation in the atomic and molecular assembly design problems at large. The present study remains a paradigm case demonstrating the advantages and capabilities of this evolutionary approach. As for the practical relevance of this study, coating the steel surfaces with Zn for corrosion resistance is a common procedure followed by numerous steel plants worldwide [21]. This study, along with its predecessors [1,2] provides a complete strategy for designing such coatings with the capability of optimum performance, which, now effectively could be scaled up for the real-life application.

References

- [1] B. Bhattacharya, G.R.D. Kumar, A. Agarwal, S. Erkoç, A. Singh, N. Chakraborti, *Comp. Mater. Sci.* 46 (2009) 821–827.

- [2] P. Rajak, U. Tewary, S. Das, B. Bhattacharya, N. Chakraborti, *Comp. Mater. Sci.* 50 (2011) 2502–2516.
- [3] N. Chakraborti, *Int. Mater. Rev.* 49 (2004) 246–260.
- [4] F. Pettersson, N. Chakraborti, H. Saxén, *Appl. Soft Comput.* 7 (2007) 387–397.
- [5] K. Sindhya, K. Miettinen, *Mater. Manuf. Process.* 26 (2011) 481–492.
- [6] D.N. Mondal, K. Sarangi, F. Pettersson, P.K. Sen, H. Saxén, N. Chakraborti, *Hydrometallurgy* 107 (2011) 112–123.
- [7] A. Schmidt, *Mater. Manuf. Process.* 26 (2011) 521–526.
- [8] K. Miettinen, *Nonlinear Multiobjective Optimization*, Kluwer, Boston, 1998.
- [9] C.A. Coello Coello, D.A. Van Veldhuizen, G.B. Lamont, *Evolutionary Algorithms for Solving Multi-Objective Problems*, Kluwer, New York, 2002.
- [10] <http://lammms.sandia.gov/>.
- [11] D. Govindan, S. Chakraborty, N. Chakraborti, *Steel Res. Int.* 81 (2010) 197–203.
- [12] A. Biswas, O. Maitre, D.N. Mondal, S.K. Das, P.K. Sen, P. Collet, N. Chakraborti, *Mater. Manuf. Process.* 26 (2011) 415–430.
- [13] V. Yamakov, D. Wolf, M. Salazar, S.R. Phillpot, H. Gleiter, *Acta Mater.* 49 (2001) 2713–2722.
- [14] J. Jeon, B. Lee, Y. Chang, *Scripta Mater.* 64 (2011) 494–497.
- [15] J. Schiotz, T. Veffe, F. Tolla, K. Jacobsen, *Phys. Rev. B* 60 (1999) 11971–11982.
- [16] A. Froseth, H. Swygenhoven, P. Derlet, *Acta Mater.* 53 (2005) 4847–4856.
- [17] N. Chakraborti, P.S. De, R. Prasad, *Z. Metallkd* 90 (1999) 508–513.
- [18] C.E. Mohn, S. Stolen, W. Køb, *Mater. Manuf. Process.* 26 (2011) 348–353.
- [19] R. Sharma, S. Nandy, P. Chaudhury, S.P. Bhattacharyya, *Mater. Manuf. Process.* 26 (2011) 354–362.
- [20] A. Kumar, D. Chakraborti, N. Chakraborti, *Steel Res. Int.* 83 (2012) 169–174.
- [21] A.R. Marder, *Prog. Mater. Sci.* 45 (2000) 191–271.